

Millimetre Wave Scattering by Spherical Hydrometeors at Selected WindSat Frequencies

Ayibapreye Benjamin¹, Ogoina Alaowei², Aguiyi Watson³

¹ Niger Delta University, Amassoma, Nigeria

² Niger Delta University, Amassoma, Nigeria

³ Federal University, Otueke, Nigeria

Abstract

This paper reports the use of Mie theory to evaluate the Mie scattering coefficients and properties of hydrometeors such as fog and sea foam by adopting the effective dielectric constants of fog and sea foam at selected WindSat frequencies. This research was implemented using MATLAB computing program by assuming the hydrometeors are spherical and homogeneous with their respective known size parameters at millimeter wavelength. The computation of Mie scattering efficiencies was achieved which have significant application in meteorology and microwave remote sensing. Plots of Mie scattering efficiencies as functions of size parameters of sea foam and fog are presented.

Keywords: Millimetre, Scattering, Homogeneous, Hydrometeors, WindSat Frequencies.

1. Introduction

Many air-sea interaction processes are quantified in terms of whitecap fraction \overline{W} because oceanic whitecaps are the most visible and direct way of observing breaking of wind waves in the open ocean. Enhanced by breaking waves, surface fluxes of momentum, heat, and mass are critical for ocean atmosphere coupling and thus affect the accuracy of models used to forecast weather and predict storm intensification and climate change. Whitecap fraction is defined as the fraction of a unit sea surface covered by foam [1]. It has been traditionally measured by extracting the high intensity pixels marking white water in still photographs or video images collected from towers, ships, and aircrafts. Satellite-based passive remote sensing of whitecap fraction is a recent development that allows long term, consistent observations of whitecapping on a global scale. The remote sensing method relies on change of ocean surface emissivity at microwave frequencies (e.g., 6 to 37GHz) due to the presence of sea foam on a rough sea surface. These changes at the ocean surface are observed from the satellite as brightness temperature $\overline{T_B}$ [1]-[2]

The algorithm to obtain \overline{W} from satellite observations of $\overline{T_E}$ was developed at the Naval Research Laboratory within the framework of WindSat mission. It improved upon the feasibility study of this remote sensing technique by using independent sources for the input variables of the algorithm, physically based models for the emissivity of rough sea surface and emissivity of foam, improved rain flag, and improved atmospheric model necessary for the atmospheric correction. The database built with this algorithm compiles \overline{W} for entire year 2006 matched in time and space with data for the wind vector, wave field (such as significant wave height and peak wave period), and environmental parameters (such as sea surface temperature and atmospheric stability). This data base has proved useful in analysing and quantifying the variability of \overline{W} . Magdalena et.al presented an updated algorithm for estimating \overline{W} from WindSat $\overline{T_E}$ data using new sources and products for the input variables. This approach replaces the originally used QuikSCAT data for ocean wind vector are replaced with new wind vector fields [3]-[4].

Xiaobin Tin et.al found large discrepancies when comparing measurements and model simulations as wind speed (WS) rise above 12ms^{-1} . Over the open ocean and for moderately wind speeds (WS_s), the Soil Moisture and Ocean Salinity (SMOS) brightness temperature ($\overline{T_E}$) was initially consistent with $\overline{T_E}$ computations made by theoretical prelaunch models implemented in European Space Level 2 Ocean Salinity processor [4]. In [4] a

new approach was proposed using new set of parameters for sea wave spectrum and foam coverage model that can be used for simulating L-band radiometer data over a large range of WS based on the deduction of wind induced components from the SMOS data.

[5]-[6] used Monte Carlo Simulation and the dense radiative transfer theory (DMRT) with quasi-crystalline approximation (QCA) to evaluate direct and inverse scattering problems. The Monte Carlo simulation use an exact numerical formulation based on Foldy-Lax multiple scattering equations of 3-D Maxwell's equation. Previous calculations assumed particles with size parameter $(ka \ll 1)$ using DMRT. An extension to moderate sized particle is vital for millimetre wave remote sensing because high frequency range above 10GHz, the particle size in geographical media is comparable to the wavelength (Mie Scattering). Contributions by Chi-Te Chan et.al shows that analytical results were consistent with Monte Carlo simulations of exact solutions of Maxwell's equations of randomly distributed finite size sphere without adjusting parameters. Input parameters of the model are all physical parameters of sizes, concentrations (volume fractions) and permittivity. The results of the models were used to obtain brightness temperatures in passive remote sensing of ocean foam at 19GHz and 37GHz.

Mie scattering could be used with QCA and QCA-CP (quasi-crystalline approximation with coherent potential) to provide solution that is consistent for particle sizes comparable to or larger than the wavelength. With results obtained from [6], the extinction behaviour of sea foam was illustrated, thermal emission from sea foam was evaluated and it was shown that the extinction was dominated by absorption. A physical model of foam emission was obtained that relates observed brightness temperature to the microstructure of foam as well as ocean surface wind vector. The brightness temperature of sea form can be presented as a function of observed angle and frequency and radiative transfer equation could be solved using derived QCA parameters.

2. Mie Theory Model of Scattering by Spherical Hydrometeors

Mie theory is unique for its ability to analyze homogeneous spheres scattering. Considering particles that are spherical having radius a with constant complex dielectric at any assumed frequency $\epsilon_c = \epsilon' - i\epsilon''$, it is essential that the relative dielectric constant of both the ratio of the particle dielectric constant and that of the medium are equivalent. Also of importance is the calculation of particles having complex chemical composition effective dielectric constant.

Diffraction oscillations and scattering effects of EM wave interactions with spherical hydrometeors can be evaluated should their optical parameters, polarization of the incident field and wavelength of the EM wave are given. The coefficients absorption, scattering, extinction and backscattering are obtainable applying Victor Raizer's model. Which is presented as

$$\{\sigma_{ext}, \sigma_{abp}, \sigma_{sca}\} = 0.74 \frac{f_v}{r_{30}} \int_0^\infty \{Q_{ext}, Q_{abp}, Q_{sca}\} r^2 N(r) dr \quad (1)$$

Where the scattering and extinction efficiencies are written mathematically as

$$Q_{sca} = \frac{2}{(ka)^2} \sum_{n=1}^\infty (2n + 1)(|a_n|^2 + |b_n|^2) \quad (2)$$

$$Q_{ext} = \frac{2}{(ka)^2} \sum_{n=1}^{\infty} (2n + 1)(|a_n|^2 + |b_n|^2) \quad (3)$$

and the absorption efficiency is obtained from equation (2) and (3)

$$Q_{abp} = Q_{ext} - Q_{sca} \quad (4)$$

Radar backscatter coefficient of scattering angle $\Theta = 180^\circ$ or $\Theta = 2\pi$ yields

$$\sigma_{bsca} = 0.74 \frac{f_v}{r_{30}} \int_0^{\infty} Q_{bsca}(r) r^2 N(r) dr \quad (5)$$

Mie coefficients a_n and b_n can be used to express absorption efficient as

$$Q_{abp} = \frac{1}{(ka)^2} \left| \sum_{n=1}^{\infty} (2n + 1)(-1)^n (a_n + b_n) \right|^2 \quad (6)$$

Mie coefficients are functions of size parameter $x = ka$ also the complex refractive index of the spherical hydrometeor. The coefficients are given as

$$a_n(x, mx) = \frac{\psi_n(mx)\psi_n(x) - m\psi_n(mx)\psi_n'(x)}{\psi_n'(mx)\xi_n(x) - m\psi_n(mx)\xi_n'(x)} \quad (7)$$

$$b_n(x, mx) = \frac{m\psi_n(mx)\psi_n(x) - \psi_n(mx)\psi_n'(x)}{m\psi_n'(mx)\xi_n(x) - \psi_n(mx)\xi_n'(x)} \quad (8)$$

Where ψ_n' and ξ_n' are the first order derivative of ψ_n and ξ_n respectively. $\psi_n(\eta)$ and $\xi_n(\eta)$ are Ricatti Bessel functions expressed as

$$\psi_n(\eta) = \sqrt{\frac{\pi\eta}{2}} J_{n+\frac{1}{2}}(\eta) \quad (9)$$

$$\xi_n(\eta) = \sqrt{\frac{\pi\eta}{2}} H_{n+1/2}^{(2)}(\eta) \quad (10)$$

$J_{n+\frac{1}{2}}(\eta)$ symbolizes the half-integral order spherical Bessel function and $H_{n+\frac{1}{2}}^{(2)}(\eta)$ the half-integral order Hankel function of second kind [7]. The amplitude functions of the scatter $(S_1(\rho), S_2(\rho))$ subsequently the scattering event for perpendicular and parallel polarizations are as follows

$$S_1(\rho) = \sum_{n=1}^{\infty} \frac{2n+1}{n(n+1)} [a_n \pi_n(\rho) + b_n \tau_n(\rho)] \quad (11)$$

$$S_2(\rho) = \sum_{n=1}^{\infty} \frac{2n+1}{n(n+1)} [b_n \pi_n(\rho) + a_n \tau_n(\rho)] \quad (12)$$

The angular Mie functions π_n and τ_n are represented by the related Legendre polynomial P_n^1 as

$$\pi_n(\rho) = \frac{1}{\sin(\Theta)} P_n^1(\rho) \quad (13)$$

$$\tau_n(\rho) = \frac{d}{d\Theta} P_n^1(\rho) \quad (14)$$

Where $\rho = \cos \Theta$

Mie's theory can be used for the calculation of the scattering, absorption, extinction cross-sections and the efficiency of single spherical hydrometeor. Evaluation of the coefficients of volume scattering, absorption and extinction coefficients also occurs when determining the size of the hydrometeor particles. These scattering boundaries are presented as follows

$$v_{sca} = \int_{r_{min}}^{r_{max}} \sigma_{sca}(r) N(r) dr \quad (15)$$

$$v_{ext} = \int_{r_{min}}^{r_{max}} \sigma_{ext}(r) N(r) dr \quad (16)$$

The single scattering albedo ω_0 an attenuated fraction of the incident EM field which is as a result of scattering in a single scattering event and is represented analytical as

$$\omega_0 = \frac{v_{sca}}{v_{ext}} \quad (17)$$

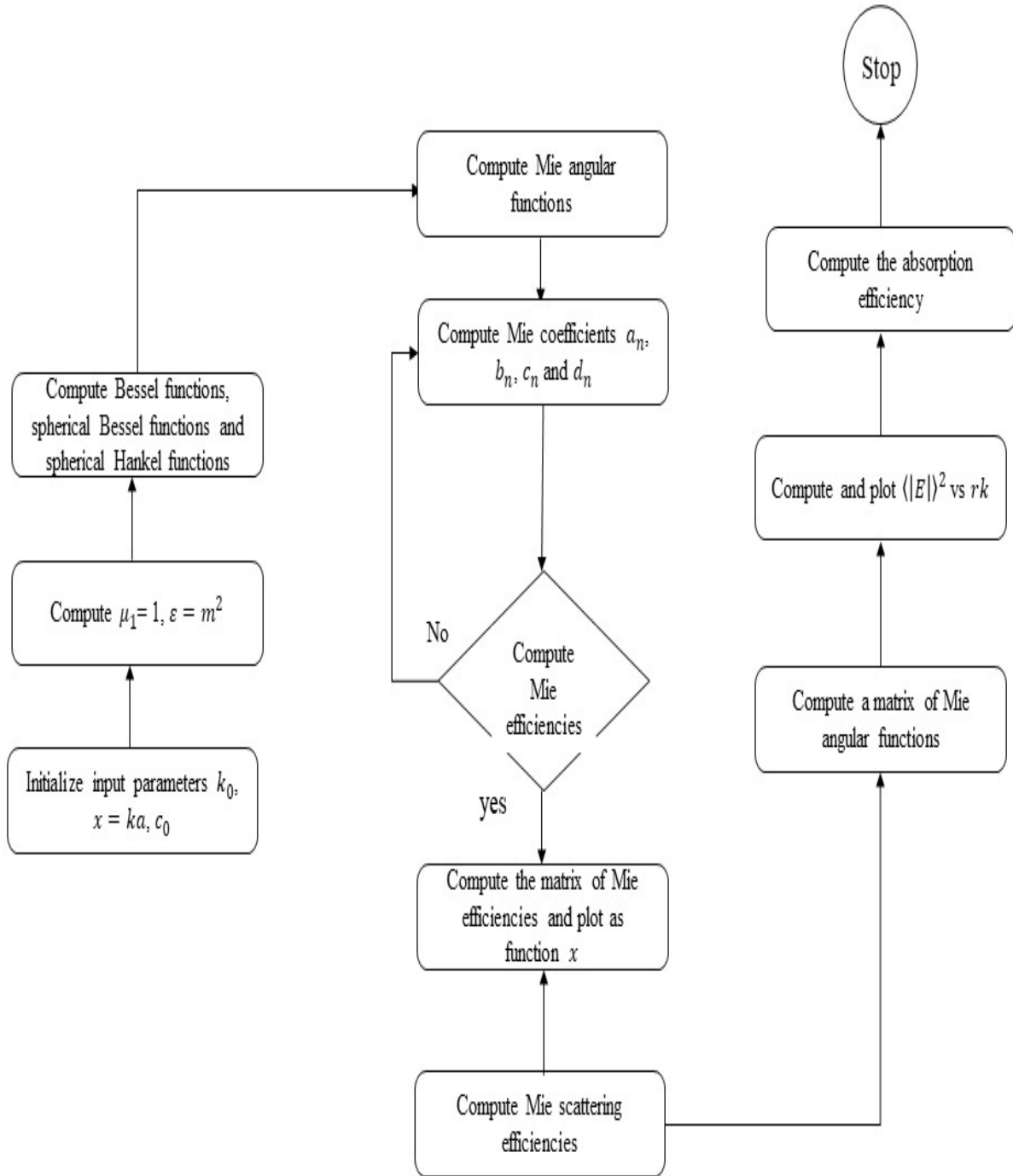


Fig. 1 Flow Chat of Mie Theory Computation

3. Results and Discussions

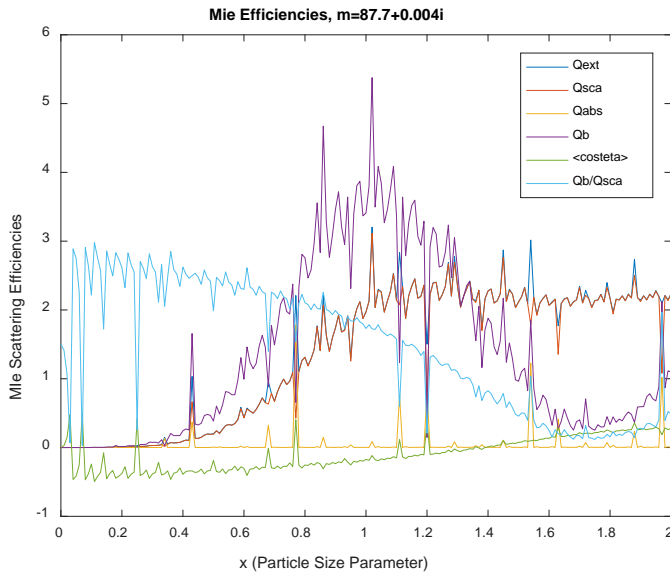


Fig. 2 Mie efficiencies for $m = 87.7 + 0.004i$ over the size parameter x range from 0 to 2 .

This shows variation of Mie scattering efficiencies with size parameter of dielectric sphere or hydrometeor (seawater). Note that the sign of $\langle \cos\theta \rangle$ changes significantly between $x \cong 0.8$ and 1.6 .

Fig. 2 illustrate that at high refractive index, the Mie scattering efficiencies are in the geometrical optics regime. The amplitude variations of the scattering efficiencies show multiple scattering due to high refractive index of the particle which are found in the geometric optics regime. When the refractive index is a complex number and the imaginary part of m is small enough ($|\text{Im}(m)| \leq 0.04$), the period of extinction ripple structure is the same as the case of m being a real number by numerical calculation. For large m , where $|\text{Re}(a_n(x, mx))|$ and $|\text{Re}(b_n(x, mx))|$ become smaller, and the amplitudes of interference oscillations decrease [7].

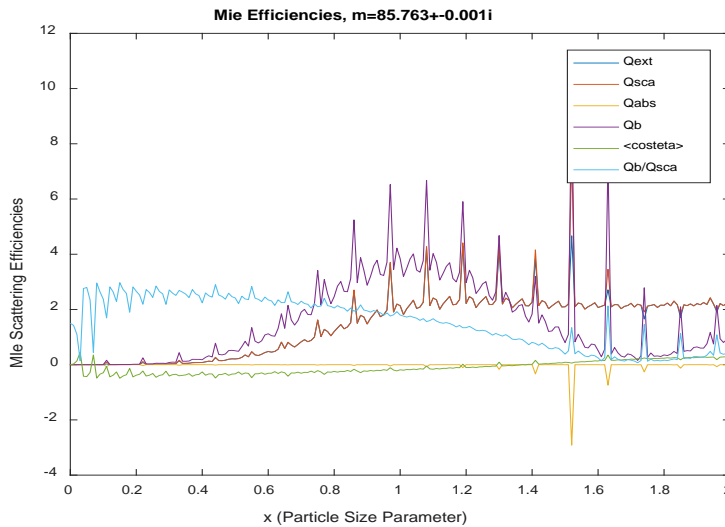


Fig. 3 Mie efficiencies for $m = 87.8 - 0.001i$ over the size parameter x range from 0 to 2 .

This shows variation of Mie scattering efficiencies with size parameter of dielectric sphere or hydrometeor. Note that the sign of $\langle \cos\theta \rangle$ changes a few times between $x \cong 1.2$ and 1.6 . The ripple structure that emerges in the extinction curve and the ripple structure has periodicity. The extinction of a light wave dispersed by a spherical particle has this important characteristic [7]. This ripple structure could be described by the extinction of the Mie sub-wave expansion formulas (equation 7) and (equation 8). The reason for the emergence of peak values of the ripple structure is the emergence of real parts of $a_n(x, mx)$ and $b_n(x, mx)$. As a result, the position of the wave structure's peak is determined by the peak value of the real component of Mie's scattering amplitude, $a_n(x, mx)$ and $b_n(x, mx)$.

This is the resonance effect

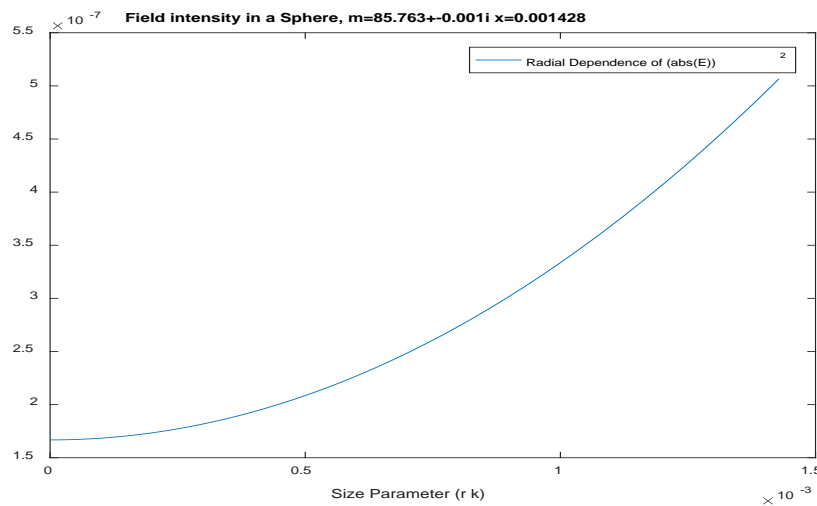


Fig. 4 Radial variation of the ratio of the internal and external absolute square electric field with refractive index and fog size parameter.

Here the field is not concentrated at the centre of the fog

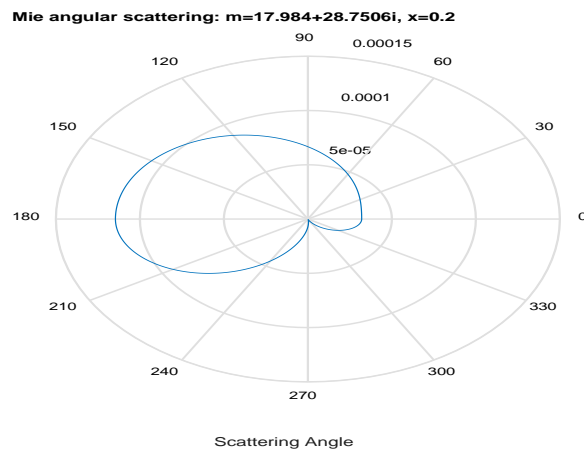


Fig. 5: Mie angular scattering by seawater at frequency 37 GHz

Angular Mie-scattering diagram of $\|S_1\|^2$ (upper Half circle) and of $\|S_2\|^2$ (lower half circle). Here, scattering in backward hemisphere is not equal to the forward hemisphere ($\langle \cos\theta \rangle = 0$), a situation mostly restricted to the region near $x = 0.2$.

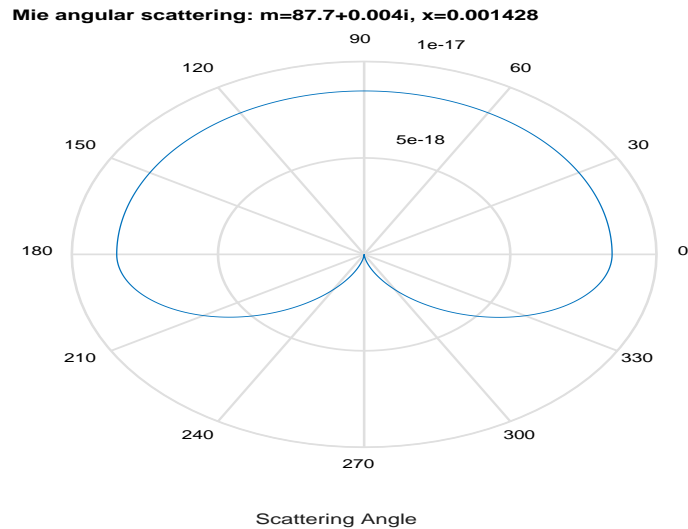


Fig. 6: Angular Mie-scattering diagram of $\|S_1\|^2$ (upper Half circle) and of $\|S_2\|^2$ (lower half circle).

Here, scattering in backward hemisphere is equal to the forward hemisphere ($\langle \cos\theta \rangle = 0$), a situation mostly constrained to the region near $x = 0.001428$.

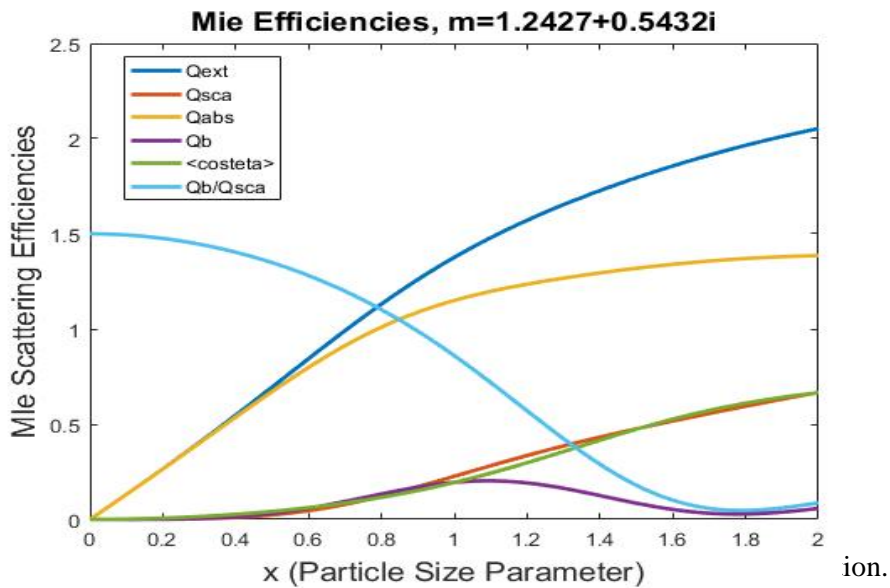


Fig. 7 Mie e

Note the sign of $\langle \cos\theta \rangle$ was constant at $x = 0$ to $x = 0.43$ and increases f between $x \cong 0.5$ to $x = 2.0$.

Fig. 7 shows that for small refractive index and diffraction parameter, the scattering efficiencies disobeys Rayleigh law for scattering by particles with size parameter of which are approximately equal to the wavelength

of radiation for the incident wave. For diffraction parameter the Mie series deviates from the Rayleigh regime and efficiency coefficients are found in the Mie scattering region [7]. The Mie series are series with a poor convergence, particularly for diffraction parameter. For large, the efficiency coefficients are in the geometrical optics regime.

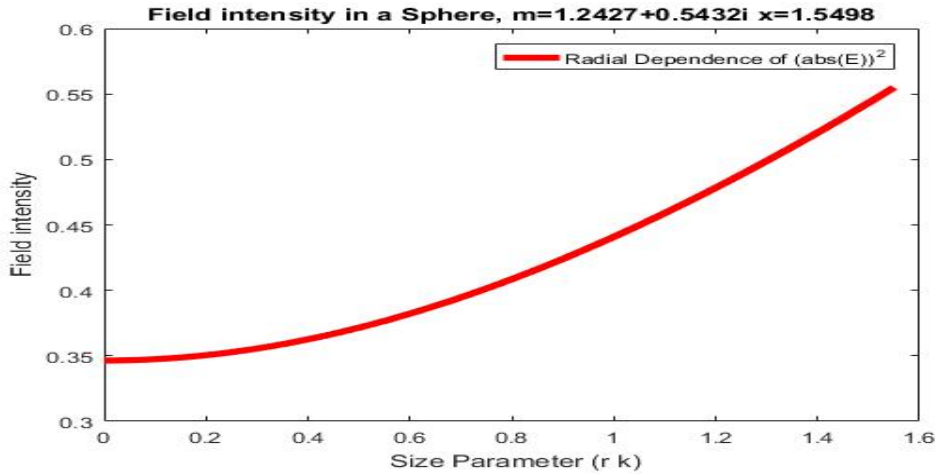


Fig. 8 Radial variation of the ratio of the internal/external absolute-square electric field with parameters $m = 1.2427 + 0.5432i$, $x = 1.5498$.

The field intensity in sea foam as a concentric sphere is not concentrated at the centre. Fig. 8 shows that the Field intensity is a function of the size parameter or diffraction parameter. It can be clearly seen that the internal field intensity increases exponentially with the size parameter of sea-foam with complex refractive index of $m = 1.2427 + 0.5432i$. For particles with large radii, the internal field in the centre of the sphere are more as compared to smaller particles. This is different from the value that is attained for the Rayleigh scattering.

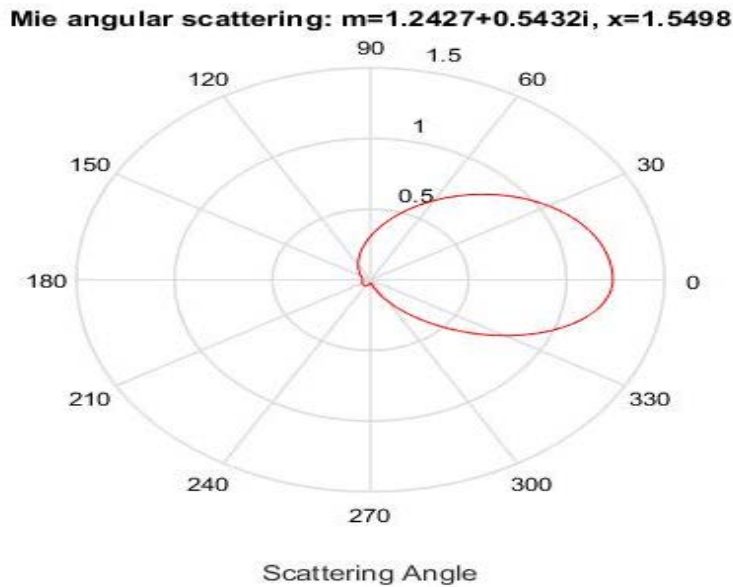


Fig 9 Mie angular scattering by sea-foam at frequency 37 GHz

Angular Mie-scattering diagram of $\|\mathcal{S}_1\|^2$ (upper Half circle) and of $\|\mathcal{S}_2\|^2$ (lower half circle). Here, scattering is minimal in the backward hemisphere as compared to that of the forward hemisphere ($\langle \cos\theta \rangle = 0$), a situation mostly constrained to the region near $\chi = 1.549$

4. Conclusions

In this paper, Gustav Mie theory was adopted for investigation of scattering properties of hydrometeors such as fog, sea water and sea foam at different frequencies and complex effective dielectric constants. By adopting the complex effective dielectric constant of sea foam and fog with their respective size parameters at millimeter wavelength, the computation of Mie scattering efficiencies was achieved which have significant application in meteorology and microwave remote sensing. The propagating electromagnetic wave (EM) was modelled using Bessel's functions, spherical Bessel's functions and Spherical Hankel functions which was utilized for the computation of Mie Scattering coefficients a_n , b_n , c_n and d_n in MATLAB computational software. Plots of Mie scattering efficiencies were made as functions of size parameters of sea foam and fog which helps to describe extinction of propagating EM wave due to its interaction with scatterers of various size parameters. Plots of Mie angular functions showed forward and backward scattering of EM wave for particles (sea foam and fog) with large and small size parameters.

Mie theory can provide excellent predictions of scattering and absorption coefficients if particle size distribution function and relative index are known. Here, scattering properties of spherical hydrometeors are computed at WindSat frequencies, these scattering parameters are significant in atmospheric studies and weather prediction.

Acknowledgments

This research work was sponsored financially by Dr. Nimibofa Ayawei.

References

- [1] M. Anguelova, M. Bettenhausen, and P. Gaiser, Passive remote sensing of sea foam using physically-based models. In *2006 IEEE International Symposium on Geoscience and Remote Sensing*, IEEE, July, 2006, (pp. 3676-3679).
- [2] M. D. Anguelova, M. H. Bettenhausen, W. F. Johnston, and P. W. Gaiser. "Passive remote sensing of oceanic whitecaps: Further developments." In *AGU Fall Meeting Abstracts*, vol. 2013, pp. A43G-0353.
- [3] Y. Xiaobin, J. Boutin, N. Martin, and P. Spurgeon. "Optimization of L-band sea surface emissivity models deduced from SMOS data." *IEEE Transactions on Geoscience and Remote Sensing* 50, no. 5 (2012): 1414-1426
- [4] Chen, Chi-Te, Jianjun Guo, Leung Tsang, Alfred TC Chang, and Kung-Hau Din. "Analytical and numerical methods for the scattering by dense media." In *IGARSS 2000. IEEE 2000 International Geoscience and Remote Sensing Symposium. Taking the Pulse of the Planet: The Role of Remote Sensing in Managing the Environment. Proceedings (Cat. No. 00CH37120)*, vol. 5, pp. 2359-2361. IEEE, 2000.
- [5] Chen, Dong, Leung Tsang, Lin Zhou, Steven C. Reising, William E. Asher, Louis Allen Rose, Kung-Hau Ding, and Chi-Te Chen. "Microwave emission and scattering of foam based on Monte Carlo simulations of dense media." *IEEE Transactions on Geoscience and Remote Sensing* 41, no. 4 (2003): 782-790.
- [6] Ao, Chi On. "Electromagnetic wave scattering by discrete random media with remote sensing applications." PhD diss., Massachusetts Institute of Technology, 2001.
- [7] Mätzler, Christian. "MATLAB functions for Mie scattering and absorption, version 2." (2002).

First Author- Dr. Ayibapreye Kelvin Benjamin, Ph. D in Computing and Electronic Systems University of Essex, United Kingdom in 2019, M.Sc. in Electronic Communications and Computer Engineering in 2010, The University of Nottingham, United Kingdom, B.Eng. Electrical/Electronic Engineering in 2006, Niger Delta University, Nigeria, a Senior Lecturer at



the Department of Electrical/Electronic Engineering, Niger Delta University, Wilberforce Island Bayelsa, Dr. Ayibapreye Kelvin Benjamin has published about 22 International Journals and Conference Papers, current research interests; remote sensing of oceanic foams and electromagnetic scattering and absorption by hydrometeors, electronic communication and computing. Dr. Ayibapreye Kelvin Benjamin is a registered member of the Council for Registration of Engineers (COREN), a registered member of Nigerian Society of Engineers (NSE) and member Nigerian Institute of Electrical/Electronic Engineers (NIEEE).

Second Author - Ogoina Alaowei is a Masters of Engineering student in the Department of Electrical/Electronic Engineering, Niger Delta University, Wilberforce Island, Bayelsa State, Nigeria.

Third Author – Aguiyi Nduka Watson, M.Eng. in Electrical Engineering, Rivers State University, Nigeria, B.Eng. Electrical Engineering, Rivers State University, Nigeria, Aguiyi Nduka Watson is an academic staff at Federal University Otueke, Bayelsa State, Nigeria and a Ph. D candidate in the Department of Electrical/Electronic Engineering, Niger Delta University, Wilberforce Island, Bayelsa State, Nigeria.